AGU PUBLICATIONS

JGR

Journal of Geophysical Research: Atmospheres

RESEARCH ARTICLE
10.1002/2015JD023565

Special Section:
Fast Physics in Climate Models: Parameterization, Evaluation, and Observation

Key Points:
- Cloud liquid inhomogeneity is described by gamma distribution shape parameter
- Shape parameter depends on scale and atmospheric instability
- Larger (smaller) shape parameter leads to more (less) cloud water in simulation

Correspondence to:
M. Zhang,
minghua.zhang@stonybrook.edu

Citation:
Xie, X., and M. Zhang (2015), Scale-aware parameterization of liquid cloud inhomogeneity and its impact on simulated climate in CESM, *J. Geophys. Res. Atmos.*, *120*, 8359–8371, doi:10.1002/2015JD023565.

Received 21 APR 2015
Accepted 25 JUL 2015
Accepted article online 29 JUL 2015
Published online 20 AUG 2015

Scale-aware parameterization of liquid cloud inhomogeneity and its impact on simulated climate in CESM

Xin Xie[1,2] and Minghua Zhang[2]

[1]Institute of Atmospheric Physics, Chinese Academy of Sciences, Beijing, China, [2]School of Marine and Atmospheric Sciences, State University of New York at Stony Brook, Stony Brook, New York, USA

Abstract Using long-term radar-based ground measurements from the Atmospheric Radiation Measurement Program, we derive the inhomogeneity of cloud liquid water as represented by the shape parameter of a gamma distribution. The relationship between the inhomogeneity and the model grid size as well as atmospheric condition is presented. A larger grid scale and more unstable atmosphere are associated with larger inhomogeneity that is described by a smaller shape parameter. This relationship is implemented as a scale-aware parameterization of the liquid cloud inhomogeneity in the Community Earth System Model (CESM) in which the shape parameter impacts the cloud microphysical processes. When used in the default CESM1 with the finite-volume dynamic core where a constant liquid inhomogeneity parameter was assumed, it reduces the cloud inhomogeneity in high latitudes and increases it in low latitudes. This is due to both the smaller (larger) grid size in high (low) latitudes in the longitude-latitude grid setting of CESM and the more stable (unstable) atmosphere. The single-column model and general circulation model sensitivity experiments show that the new parameterization increases the cloud liquid water path in polar regions and decreases it in low latitudes. An advantage of the parameterization is that it can recognize the spatial resolutions of the CESM without special tuning of the cloud water inhomogeneity parameter.

1. Introduction

The physical parameterizations of subgrid processes are crucial for realistic climate simulation in climate models. They are usually designed based on physical assumptions with empirically determined parameters. Because the subgrid processes depend on the size of the model grids, these parameters need to be tuned for different resolutions of the model. Tuning a model is not only tedious but also difficult when variable resolutions of drastically different grid sizes need to be used, such as the regional refinement of grids [*Taylor et al*., 2008]. Therefore, it is of great interest to develop scale-aware parameterizations to make them resolution independent.

The subgrid variability of cloud hydrometers is known to impact radiation and microphysics processes in climate models. It was introduced into the general circulation models (GCMs) in *Cahalan et al*. [1994] and *Barker* [1996] to correct the radiation flux biases over horizontally inhomogeneous clouds. Relative to homogeneous clouds, the subgrid-scale variability of cloud water reduces the grid-averaged albedo of solar radiation. The inhomogeneity of cloud water within a grid cell also leads to more efficient conversion of liquid water to rainwater because of the nonlinear dependence of the conversion rate on liquid water content [e.g., *Morrison and Gettelman*, 2008]. Several methods have been used to describe the subgrid variability of cloud water in large-scale models. Some studies represented it with the subcolumn method, which statistically reconstructs the internal cloud structure by using large-scale cloud fraction information and overlapping assumption [*Jakob and Klein*, 1999, 2000; *Jess et al*., 2011; *Pincus and Stevens*, 2009; *Pincus et al*., 2003, 2006; *Raisanen et al*., 2004]. Other studies sought to specify the assumed probability density function (PDF) of cloud quantities diagnostically or prognostically [*Bogenschutz and Krueger*, 2013; *Golaz et al*., 2002; *Larson and Golaz*, 2005; *Norris et al*., 2008; *Tompkins*, 2002] so that the subgrid variability effect can be accounted by integrating the cloud PDF for microphysics [*Larson and Griffin*, 2013; *Pincus and Klein*, 2000; *Weber and Quaas*, 2012; *Wood et al*., 2002] and radiation calculations [*Shonk and Hogan*, 2008, 2010; *Shonk et al*., 2010].

Previous studies have pointed out the strong dependence of subgrid variability on the horizontal scale and other atmospheric conditions. However, few studies have investigated in how to quantitatively describe these dependences. *Pincus et al*. [1999] related the cloud subgrid variability to the underlying cloud types.

Oreopoulos and Cahalan [2005] gave a very comprehensive survey for the 1° × 1° global cloud inhomogeneity climatology including latitudinal, seasonal, and diurnal changes using Moderate Resolution Imaging Spectroradiometer (MODIS) data. *Kawai and Teixeira* [2011] examined the probability density function of marine boundary layer clouds and pointed out its implications for cloud parameterization. These studies provided very valuable observational basis to formulate cloud inhomogeneity, even though they did not directly derive the cloud inhomogeneity parameterizations for large-scale models. *Hogan and Illingworth* [2003] was the first study that described a linear empirical relationship of ice water content inhomogeneity on grid size and vertical shear of the horizontal wind from cloud radar observations. *Hill et al*. [2012] provided another parameterization for the horizontal inhomogeneity of ice water content based on a nonlinear relationship on horizontal scales and cloud amount. *Boutle et al*. [2013] extended the *Hill et al*. [2012] formulation to liquid water content and precipitation. These two recent parameterizations used both cloud fraction and horizontal scale as the predictor variables. Our study differs from theirs by keeping the nonlinear scale relationship but including other meteorological conditions. According to *Kawai and Teixeira* [2011], the in-cloud liquid inhomogeneity should also depend on atmosphere instability, which will be used in the parameterization derivation of this study.

The objective of this paper is to use the long-term high-resolution data of cloud water from the Department of Energy (DOE) Atmospheric Radiation Measurement Program (ARM) at different latitudes to develop a scale-aware parameterization of cloud water inhomogeneity on resolved atmospheric instability. A second objective is to understand the impact of the parameterization on the simulated climate by the Community Earth System Model (CESM). Recently, *Huang et al*. [2014] used the same data set to study the standard deviation, relative dispersion (the ratio of the standard deviation to the mean), and skewness of cloud liquid water. They reported the dependence of these parameters on the length of the averaging time. Our work differs from their study in that we focus on the dependences on the spatial length scale and the atmospheric conditions, and we target them for parameterizations in large-scale models. An outline of this paper is as follows. Section 2 describes the observational data and methods that we use to estimate the liquid cloud inhomogeneity. Section 3 shows the relationship of the cloud inhomogeneity parameter with scale, location, and season. A parameterization is presented. Section 4 presents the results of the impact of the new parameterization in CESM single-column and general circulation model (GCM) experiments. Section 5 contains a summary.

2. Data and Model

This study uses the ground-based Climate Research Facility Continuous Baseline Microphysical Retrieval (MICROBASE) value-added product developed by ARM [*Johnson and Jensen*, 2011]. MICROBASE combines measurements from 35 GHz millimeter wavelength cloud radar, ceilometer, micropulse lidar, microwave radiometer, and balloon-borne radiosonde soundings to produce cloud water vertical profile [*Johnson et al*., 2011]. Its latest version MICROBASEPI2 provides instantaneous liquid water content profile in 10 s time intervals and 512 vertical levels, each layer 43 m thick. The resultant temporal resolution is sufficient to capture the small-scale cloud profile for the present study of cloud variability. The quality control flags supplied by the product classify the liquid data into bad, indeterminate, and good categories. The good flag has excluded many questionable measurements, for example, liquid water content out of normal range or with precipitation contamination, so only the liquid water content data with good quality flag are used in this study. As a common problem for cloud radar reflectivity data, drizzle may introduce positive bias to liquid water content in lower altitude and this could result in some uncertainty in parameterization derivation. But since cloud variability usually measures the ratio of cloud water content mean to its variance (shown later in equation (2)), the error introduced by incorrect scaling in lower levels should be less. Because our focus is only on in-cloud liquid inhomogeneity, only the data with liquid water content greater than zero are used. Data from the ARM sites at Barrow (NSA C1), Lamont (SGP C1), and Darwin (TWP C3) are selected to represent high, middle, and low latitudes, respectively. To demonstrate the capability of MICROBASEPI2 data set, Figure 1 gives two examples of short-term MICROBASEPI2 temporal variation of liquid water content above two of the ARM sites. Figure 1a shows middle and low clouds at SGP C1, while Figure 1b shows deep convective clouds at TWP C3. With the high temporal 10 s resolution, the data reveal more small-scale details in the liquid cloud distributions.

To study the spatial scale dependence of liquid cloud inhomogeneity, the ground-based MICROBASE cloud measurements in temporal coordinate cannot be used directly. We have to assume the ergodicity of clouds

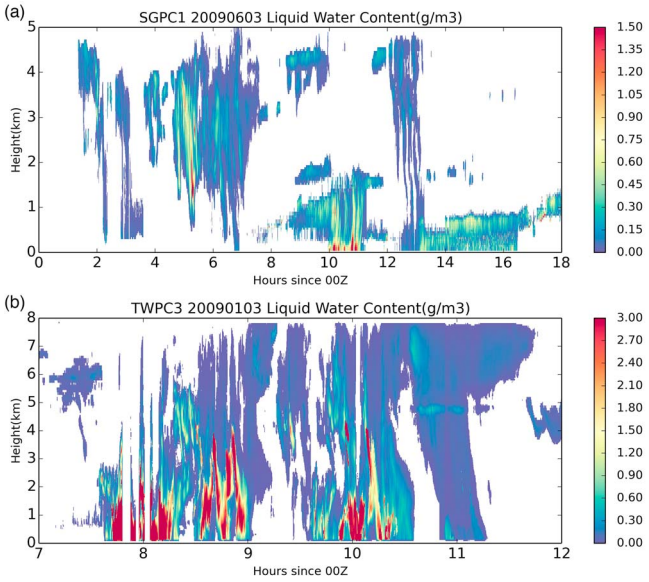

Figure 1. (a) An example of MICROBASEPI2 liquid water content profile on 3 June 2009 at SGP C1 site. (b) Same as Figure 1a but at TWP C3 site on 3 January 2009.

so that the spatial variability can be deduced with the cloud data and wind data combined. *Grützun et al*. [2013] suggested that the ergodicity assumption of ground-based remote sensing data may introduce bias for cloud spatial variability studies within a short time period. Therefore, we used 3 years of long-term data (from 2008 to 2010) in this paper to alleviate that bias. Wind velocity from the ARM Best Estimate data product [*Xie et al*., 2010], with vertical resolution 45 m and 6 h temporal interval, is then integrated respectively at each vertical level to calculate what distance the cloud field has flowed over. This transformation converts the temporal variation into spatial distribution.

In spatial coordinate, we quantify the in-cloud liquid cloud inhomogeneity by using the shape parameter ν of a gamma distribution at different spatial scales. The same gamma distribution is used in the cloud microphysical scheme of CESM [*Morrison and Gettelman*, 2008] to calculate the autoconversion and collision-coalescence processes of cloud droplets with a specified value of 1.0 for the shape parameter. A gamma distribution is assumed because it has been found to fit observational cloud water well [e.g., *Barker et al*., 1996; *Huang et al*., 2014]. The gamma distribution is written as

$$P(q) = \frac{1}{\Gamma(\nu)} \frac{1}{\theta^{\nu}} q^{\nu-1} e^{-\frac{q}{\theta}} \tag{1}$$

where ν is the shape parameter and θ is the scale parameter. The shape parameter ν in the gamma function can be written as

$$\nu = \frac{\overline{q}^2}{\sigma^2} \tag{2}$$

where σ^2 is the variance of in-cloud liquid water mixing ratio q and $\overline{q}$ is the mean of q. The shape parameter ν of liquid water is calculated using maximum likelihood method (MLE) [*Thom*, 1958] from the MICROBASE data for clouds of different spatial scales (including both clear-sky and cloudy conditions). Every four vertical levels of MICROBASE data are combined as one level, in order to obtain more liquid samples to do distribution estimation. The ARM Best Estimate data set (ARMBE) is also used in the derivation of the parameterization to understand which atmospheric condition controls ν.

Note that several other measures could be used to characterize cloud inhomogeneity, for example, inhomogeneity parameter χ [*Oreopoulos and Cahalan*, 2005] or fractional standard deviation f [*Boutle et al*., 2013; *Hill et al*., 2012]. These parameters are generally comparable and can be converted to each other [*Shonk et al*., 2010]. The reason we use the definition of inhomogeneity in terms of ν in this paper is that CESM also uses ν to represent liquid cloud inhomogeneity in microphysics conversion process [*Gent et al*., 2011; *Morrison and Gettelman*, 2008]. We are interested to implement the scale-aware parameterization of ν in CESM and investigate its impact on simulated climate. We also use the single-column version of CESM to analyze the impact. In the single-column setting, we run a short simulation at SGP C1 to evaluate the direct impact of ν on simulated cloud water without its interactive effect on radiation and microphysics. In the GCM configuration, we run the CESM stand-alone atmospheric model CAM5 with prescribed climatological sea surface temperatures (SSTs) at a 2° longitude-latitude grid with the finite-volume dynamical core. Since the longitude-latitude grid in CESM has larger (smaller) horizontal size over equator (polar region), the scale impact of the parameterization could be investigated. We run each simulation for 4 years and analyze the results from the last 3 years.

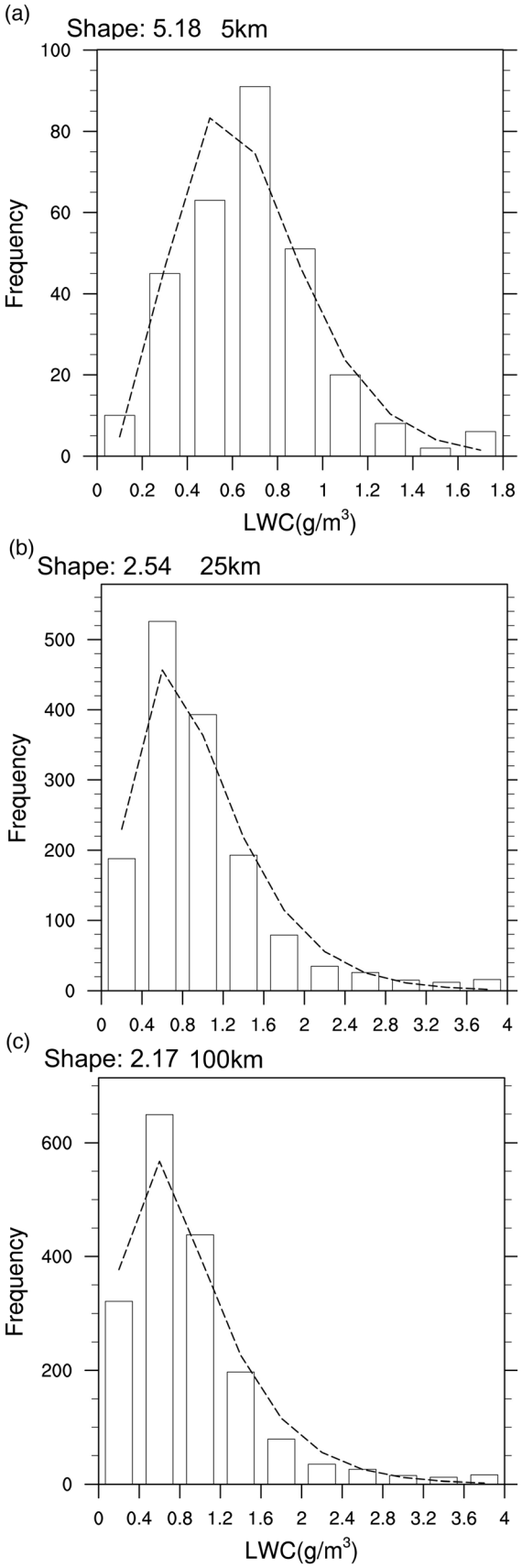

3. Parameterization of the Shape Parameter

3.1. Shape Parameter Dependence on Scales and Atmosphere Instability

At each location and height, the frequency distribution of the in-cloud liquid water is obtained from the high-resolution data within the given scale. Figures 2a–2c show the examples of the frequency distribution at SGP C1 and at 100 m height for three different horizontal scales (5 km, 25 km, and 100 km, respectively) at about 02Z on 3 June 2009. Also plotted is the fitted gamma distribution (dashed lines) using MLE. It can be seen that the gamma distributions capture the shape of the observed liquid water content histogram well. We can also see that the estimated shape parameter from the fitting decreases (from 5.18 to 2.17) with the increasing horizontal scales (from 5 km to 100 km). This is because a spatial segment of larger scale tends to cover more cloud regimes so it includes more liquid inhomogeneity than a smaller scale. Therefore, larger scales are associated with larger variance of liquid water for the given mean liquid water, so they are associated with smaller shape parameter (see equation (4)). Smaller scales, however, may just cover a portion of a large cloud. They are associated with larger shape parameter. As the scale approaches zero, the variance of liquid water will approach zero, which is associated with an infinite shape parameter.

We calculated the shape parameters for different sites (NSA C1, SGP C1, and TWP C3), different seasons (December-January-February (DJF) and June-July-August (JJA)), and different scales (from 5 km to 200 km). The median values at each height are shown in Figure 3 in dense lines, with the three locations given in the three rows, the two seasons given in the two columns, and the

Figure 2. Examples of the frequency distribution of cloud water and the gamma distribution fitting using the maximum likelihood method. The data are from the ARM SGP on 3 June 2009 in Figure 1 at 100 m height. The sampling horizontal scales are (a) 5 km, (b) 25 km, and (c) 100 km.

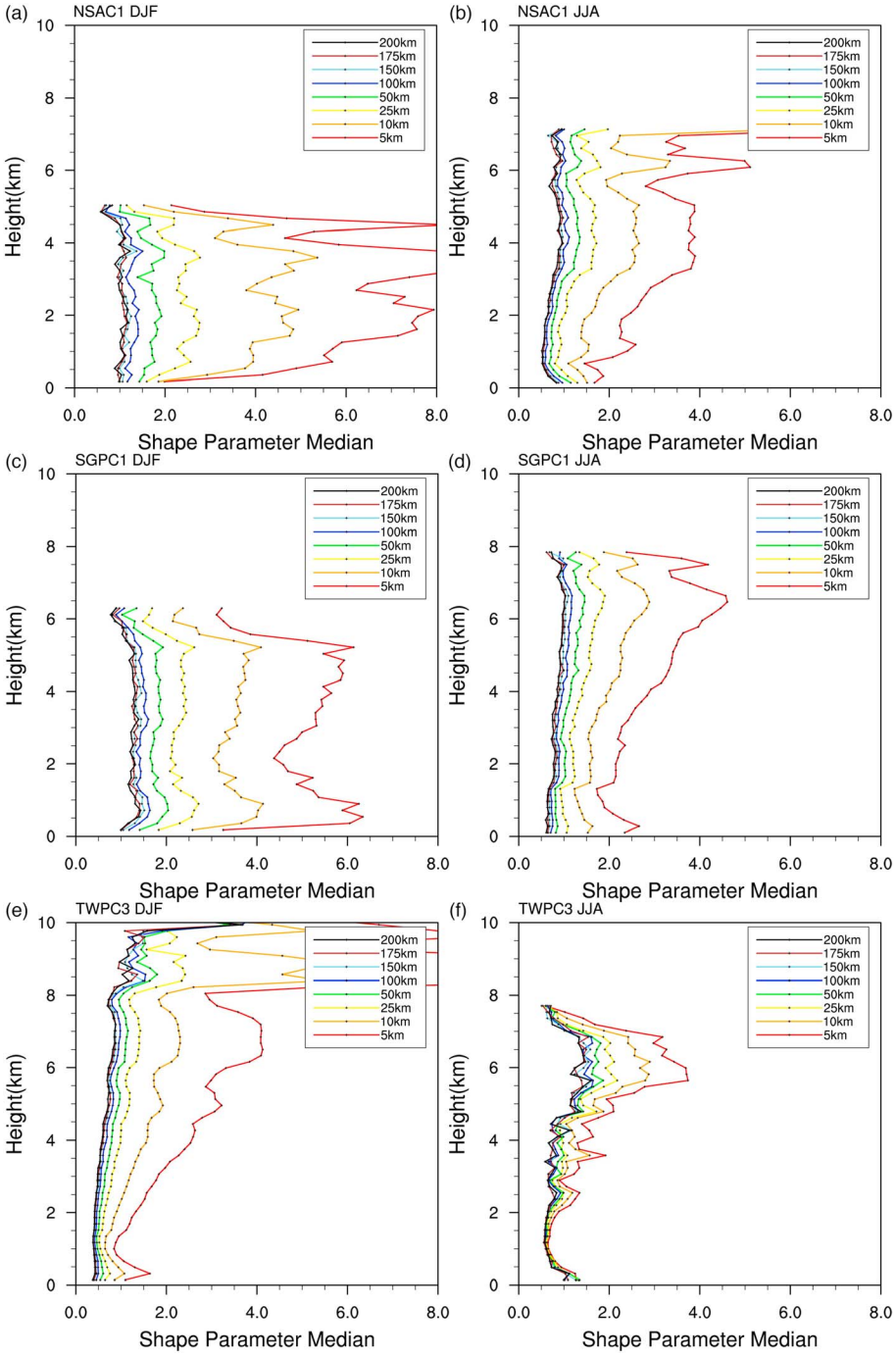

Figure 3. The shape parameter for NSA C1, SGP C1, and TWP C3 sites in DJF and JJA. Different colors represent different scales as shown in the legend.

various scales in different colors. Several features are noted. The first is the consistent decrease of the shape parameter with increasing horizontal scales in almost all the panels. The decrease is not linear. For example, in Figure 3a, the shape parameter changes from around 5 to 2 for small scales from 5 km to 50 km while for larger scales from 50 km to 200 km, the change is only from 2 to 1.

The second feature in Figure 3 is that ν depends strongly and consistently on seasons and locations. At NSA and SGP, ν in JJA is systematically smaller than its magnitude in DJF, meaning more inhomogeneity in the warm season. From the high-latitude NSA C1 to the low-latitude TWP C3, the shape parameter also shows

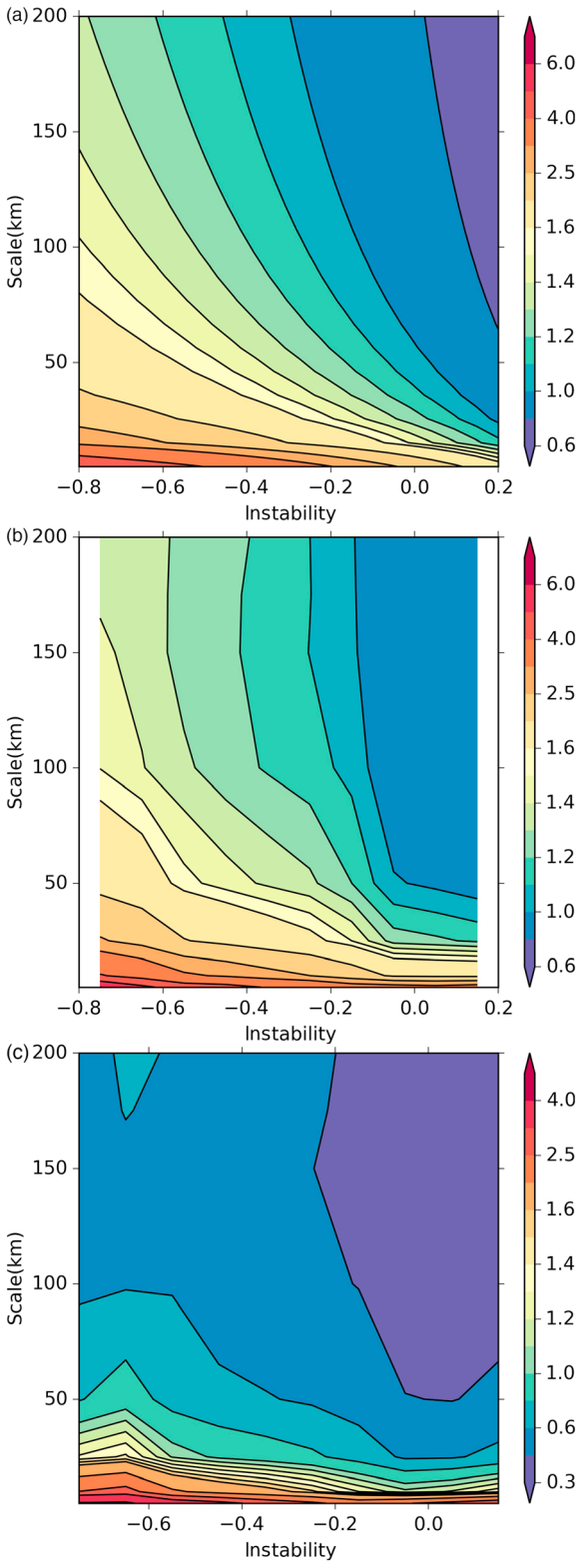

Figure 4. (a) The parameterized shape parameter as a function of scale and atmospheric instability. (b) The binned mean of observational shape parameter as a function of scale and atmospheric instability. (c) The binned standard deviation of the random term estimated from observations.

consistent decreasing trend. This is likely because the low-latitude and warm atmosphere is more frequently associated with more unstable atmospheric condition and convective clouds than the high-latitude and cold atmosphere; thus, it has larger inhomogeneity and smaller shape parameter. The dependence of seasons and locations here is consistent with the results of *Kawai and Teixeira* [2011]: more (less) cloud inhomogeneity in warm (cold) season. They also found the relationship between the cloud inhomogeneity and atmospheric instability. Based on these observations, we combine the shape parameter dependences on season and location into one single variable, atmosphere instability, for any given scale.

There is also a height dependence of the shape parameter in Figure 3. However, no systematic relationships with height can be derived for all stations. We therefore neglect the height dependence of ν, acknowledging that this can be improved in the future.

3.2. Parameterization

A simple metric of atmosphere instability can be defined as

$$S = \frac{h_{950} - h^*_{500}}{45,000Pa} \tag{3}$$

where h_{950} is the moist static energy at 950 hPa and h^*_{500} is the saturated moist static energy at 500 hPa. This formula is an approximate measure of convective available potential energy, but its simplicity allows for easy calculations [*Arakawa and Schubert*, 1974]. Usually, the larger the S, the more unstable the atmosphere is. This instability parameter is calculated using the data from ARMBE. When S is negative, the atmosphere is usually stable. S is a crude measure of the atmospheric stratifications.

According to the previous studies [*Boutle et al.*, 2013; *Hill et al.*, 2012], the nonlinear dependence of scale on cloud inhomogeneity can be described by a −5/3 power law relationship. In their papers, cloud inhomogeneity is represented by fractional standard deviation

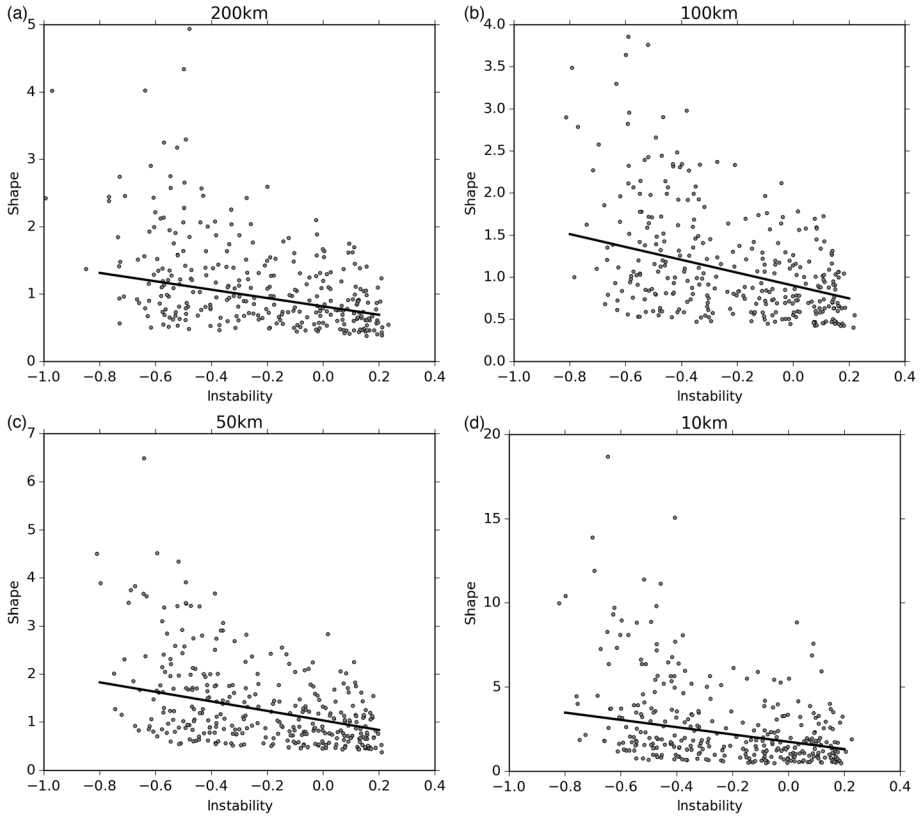

Figure 5. Parameterized shape parameter (black solid line) versus observationally derived lower quartile, median, and upper quartile of the shape parameter (gray dots) in each month as a function of atmospheric instability for different horizontal scales: (a) 200 km, (b) 100 km, (c) 50 km, and (d) 10 km.

$f = \sigma/\overline{q}$, which is proportional to $x^{1/3}$ (x is length scale). We follow their proposed scale power in this paper. Since we use shape parameter ν to represent inhomogeneity here, the relationship of $\nu = 1/f^2$ implies that the equivalent scale power for ν is $x^{-2/3}$. Multivariate regression method was then used to find the best fit of ν as a function of the scale $x^{-2/3}$ and the atmosphere instability S at the three latitudes and in the two seasons. We arrived at the following formula:

$$\nu = 0.67 - 0.38 \cdot S + 4.96 \cdot x^{-\frac{2}{3}} - 8.32 \cdot S \cdot x^{-\frac{2}{3}} + R(x, S) \tag{4}$$

where the horizontal scale x is in kilometer, S is atmospheric instability given in equation (3) in J/kg/Pa, and R is a stochastic parameter to represent the uncertainties of the ν values from cloud variability, including the sampling errors and the imperfectness of the formula. We note that the two dependent parameters and the form of the parameterization are only heuristically determined because of the inherent complexities of the cloud variability. This formula is plotted in Figure 4a with S as the abscissa and the scale as the ordinate with $R(x, S)$ set to zero. As expected, shape parameter decreases with increasing horizontal scale and increasing atmospheric instability. Figure 4b shows the binned mean of shape parameter from observation. It is seen that equation (4) captures the major pattern of ν variations in observations, especially for scales smaller than 90 km. It may underestimate ν at large scales slightly (in the upper region of the figure) compared with the binned observational mean, but this is still within the observational range. The standard deviation of the random term $R(x, S)$ is shown in Figure 4c.

To further investigate whether the parameterization can reflect the realistic variability of shape parameter in observation, we have included Figures 5a–5d to show the shape parameters from the instantaneous observations against the corresponding values from the parameterization with the stochastic term set to zero, for different given scales. For 3 years of data, we have collected the lower quartile, the median, and the upper quartile of the instantaneous ν respectively in each month and calculated the parameterized ν based on the collocated instability and spatial scale using equation (4). In these figures over the selected horizontal

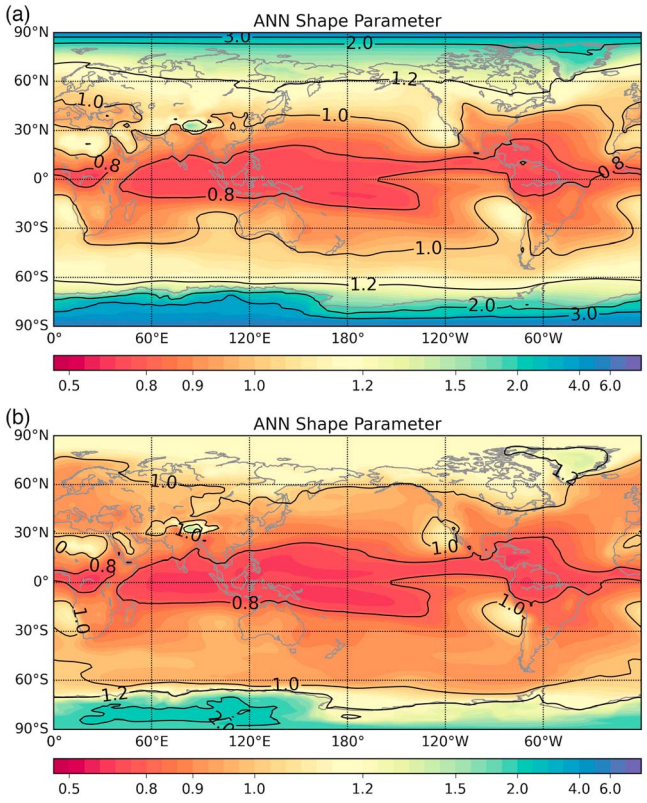

Figure 6. (a) Annual mean of global shape parameter distribution diagnosed from CESM simulation using a 2° × 2° resolution. (b) Same as Figure 6a but assuming a global 200 km spatial scale.

scales, the observational shape parameters (shown as dots) exhibit a significant decrease with larger instability (more unstable atmosphere), which is well captured by the derived parameterization shown in solid black line. The scale dependence is also evident. The overall magnitude of ν changes from about 1.0 for 200 km to about 4.0 for 10 km (see Figures 5a and 5d), and the parameterization lies within the observational range. The unresolved variability is represented by the residual term $R(x, S)$ in equation (4), which is shown in Figure 4c. When the shape parameter is used in the microphysical parameterization, this residual term can either be set to zero or treated stochastically to represent the uncertainties.

4. Impact on Climate Simulations

The proposed parameterization is next implemented in CESM for the calculation of cloud microphysics. In the global model, at the location where the surface pressure is lower than 950 hPa, h_{950} is replaced by the surface moist static energy and the denominator is replace by ($P_s - 50{,}000$ Pa) in equation (3), where P_s is surface pressure. Figure 6a shows the global distribution of the annual mean shape parameter diagnosed from CESM simulation in 2° × 2° resolution. It is seen that ν gradually increases from about 0.7 in the equatorial regions to up to 5.0 in the polar regions. This is consistent with the longitude-latitude grid size distribution in CESM, where the larger low-latitude grid size contains more inhomogeneity (lower ν) and vice versa. Along the same latitude band, atmosphere instability also plays a significant role in varying ν, especially in the tropics. The area with lower ν generally matches the region with high SST and convective clouds, such as Tropical West Pacific Warm Pool, the Pacific Intertropical Convergence Zone (ITCZ), and the Atlantic ITCZ.

Some previous studies also provided the map for the global distribution of ν [*Lebsock et al.*, 2013; *Oreopoulos and Cahalan*, 2005]. The spatial pattern of our parameterized shape parameter is consistent with *Lebsock et al.* [2013], where major tropical oceans usually have lower ν and high latitudes have larger ν (see their Figure 6).

Table 1. Comparison of Cloud Inhomogeneity Parameters With Previous Studies[a]

Reference, Source	Observational Property	Effective Spatial Resolution	Grid Box Size	Estimation Method	Mean of Equivalent ν
Barker [1996], Landsat	cloud optical depth	0.04 km	58 km	MOM	1.5
Oreopoulos and Cahalan [2005], MODIS	cloud optical depth	2 km in middle latitude and 5 km in equator	1° × 1°, 45 km in middle latitude, and 110 km in equator	MLE and MOM	2.96 in Jan and 2.87 in Jul
Lebsock et al. [2013], CloudSat and MODIS	cloud water path	1.1 km	141 km	MOM	2.46
Parameterization in this study, MICROBASE	liquid water content	0.01 km to 0.1 km for wind speed 1 m/s to 10 m/s	2° × 2°, 90 km in middle latitude, and 220 km in equator	MLE	1.1

[a]The references may have different inhomogeneity definition usually estimated by either MOM (method of moments) or MLE (maximum likelihood estimation), but we have converted them to the equivalent gamma shape parameter ν.

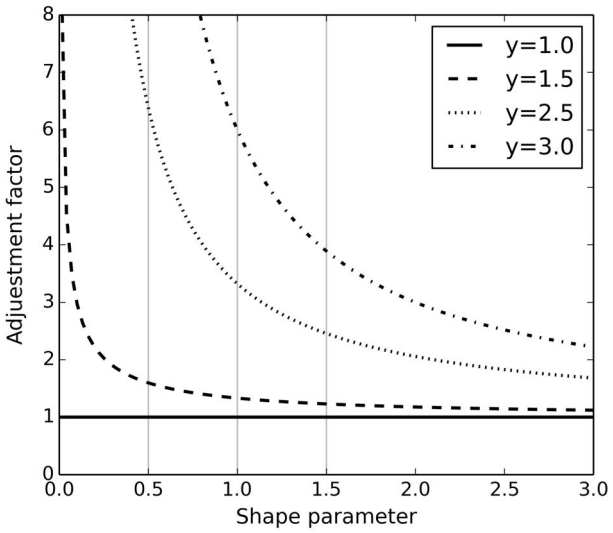

Figure 7. The adjustment factor in the conversion rate of microphysics scheme with different power relations ($y = 1, 1.5, 2.5, 3$).

The magnitude of our parameterized v is overall smaller than most previous studies based on satellite data [*Barker*, 1996; *Boutle et al*., 2013; *Cahalan et al*., 1994; *Lebsock et al*., 2013; *Oreopoulos and Cahalan*, 2005]. In Table 1, we compared the cloud inhomogeneity parameter values and the different sampling methods from these studies as summarized by *Shonk et al*. [2010] with our study. The relatively smaller value in our study is likely because we used radar data at high temporal and vertical resolutions while these studies used satellite cloud optical depth data. Higher-frequency sampling captures more cloud variability and may introduce larger variance σ^2 therefore causing smaller v ($v = \overline{q}^2/\sigma^2$). Our result is comparable to *Barker* [1996] (Table 1), which uses Landsat data with 0.04 km sampling resolution, higher than other satellite studies in the table. In addition, the larger grid box size using a CESM $2° \times 2°$ grid in our study is mostly larger than the horizontal scale they did estimation from (see Table 1). Therefore, more inhomogeneity and smaller v is expected.

In the microphysical scheme of CESM, prior to version 1.2.0 [*Morrison and Gettelman*, 2008], v was set as 2.0, which is closer to the overall mean v from *Lebsock et al*. [2013] and *Oreopoulos and Cahalan* [2005]. It has been changed to 1.0 in the publically released default model of CESM version 1.2.0, closer to our estimation. From Figure 6a, we can see that the parameterized v could be from about 0.7 with 200 km grid box over equatorial unstable atmosphere to about 5.0 with much smaller grid box at the polar region. Therefore, according to the parameterization, the default fixed value 1.0 overestimates v at low latitudes but underestimates it at high latitudes. The use of grid with uniform spatial grid box size may greatly reduce such large cloud inhomogeneity difference due to scale dependence. We have also included a map of v distribution assuming global constant spatial scale 200 km in Figure 6b to emulate such uniform grid. Note that the color scale in Figure 6b covers a much smaller range than that in Figure 6a. The spatial variation of v in Figure 6b is entirely due to changes in atmospheric conditions. At high latitudes, v is still larger, but the latitudinal gradient of v is reduced.

As has been pointed out in many previous studies [e.g., *Huang and Liu*, 2014; *Lebsock et al*., 2013], the shape parameter v can impact the conversion rates in the sources and sinks of the cloud liquid water. When the source or sink terms S is expressed as liquid water mixing ratio q_l to the power of y as $S \propto (q_l)^y$, the subgrid variability effect can be described by multiplying the conversion rate with an adjustment factor [*Morrison and Gettelman*, 2008]:

$$E = \frac{\Gamma(v+y)}{\Gamma(v)v^y} \tag{5}$$

Figure 7 shows how the adjustment factor changes with v within commonly used y range (from 1.0 to 3.0) in the microphysical schemes. Compared with the globally fixed shape parameter 1.0 in the default CESM, a ±0.5 change of shape parameter around 1.0 could introduce about ±20% change to the original adjustment factor given $y = 1.5$ and more than about ±120% change given $y = 3$. In CESM, the major nonlinear conversion terms in the liquid water tendency equation are from the rain autoconversion and accretion processes, with y values of 2.47 and 1.15, respectively [*Khairoutdinov and Kogan*, 2000; *Morrison and Gettelman*, 2008]. Therefore, compared with the fixed v 1.0 case, the parameterized v will lead to higher conversion rate from cloud liquid to rain in the low latitudes ($v < 1.0$) and lower conversion rate in the higher latitudes ($v > 1.0$).

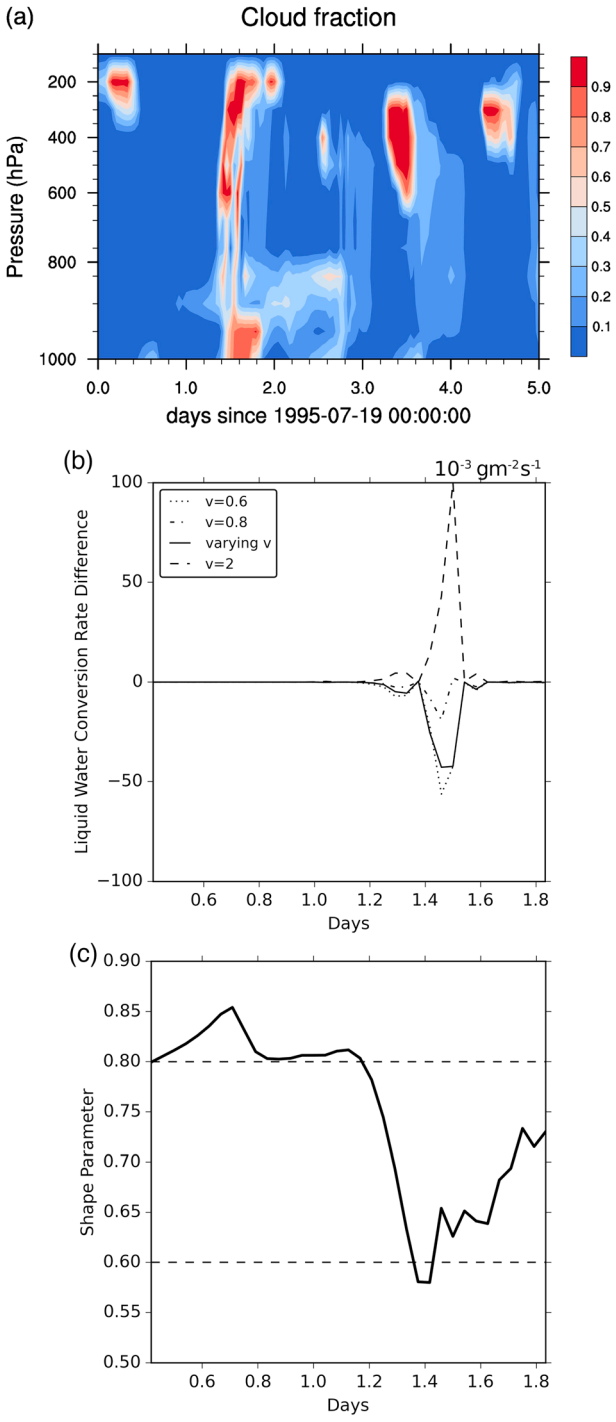

Figure 8. (a) Cloud fraction from a 5 day simulation from the single-column simulation of CAM5. (b) Column-integrated microphysics liquid water conversion difference by using shape parameters $\nu = 0.6$, $\nu = 0.8$, $\nu = 2.0$, and parameterized varying ν relative to the control simulation of $\nu = 1.0$. (c) The corresponding varying ν magnitude.

4.1. Single-Column Simulation

We first use a single-column simulation to demonstrate the direct impact of ν on CESM microphysics processes. The simulation uses ARM SGP forcing data starting on 19 July 1995 for 5 days. The control run uses CESM default setting with the fixed $\nu = 1.0$. Figure 8a shows the cloud fraction distribution from the control run. Convection developed at the day 1.5, so significant microphysical conversion from liquid cloud to precipitation is expected at that moment. Focusing on this short period of vigorous cloud activity, we carried out the offline microphysics calculation with $\nu = 0.6$, $\nu = 0.8$, $\nu = 2.0$, and the CESM $2° \times 2°$ grid scale. The interactive effect of ν is suppressed by using the liquid water from the control run in the radiation and in the subsequent microphysical calculations. The lines in Figure 8b show the liquid water conversion difference within each time step between the sensitivity simulations and the one from the control run. As expected, the simulations with ν smaller than 1.0 shown by dotted line ($\nu = 0.6$) and dash-dotted line ($\nu = 0.8$) have larger liquid water sinks (more negative tendency). But the one with $\nu = 2.0$ has more liquid water due to smaller liquid water conversion. The difference in the liquid water tendency from the simulation using the parameterized ν is shown by a solid line. It is between the lines using $\nu = 0.6$ and $\nu = 0.8$ at the peak. The corresponding ν is plotted in Figure 8c as the thick line that fluctuates around 0.7. These are all consistent with the expectation that smaller ν, corresponding to large inhomogeneity of liquid water, is associated with larger cloud-to-rain conversion rate, and less cloud water, while the opposite is true for larger ν.

4.2. GCM Simulation

We next show the sensitivity of the cloud liquid water to the varying ν using GCM simulation. Instead of fixing liquid water content and diagnosing its converting tendency offline, we calculated the parameterized shape parameter ν at each grid point of CESM and allowed it to impact the microphysics processes in the *Morrison and Gettelman* [2008] cloud microphysical scheme. The liquid water content will respond to the modified cloud liquid conversion rates, so liquid cloud distribution will be

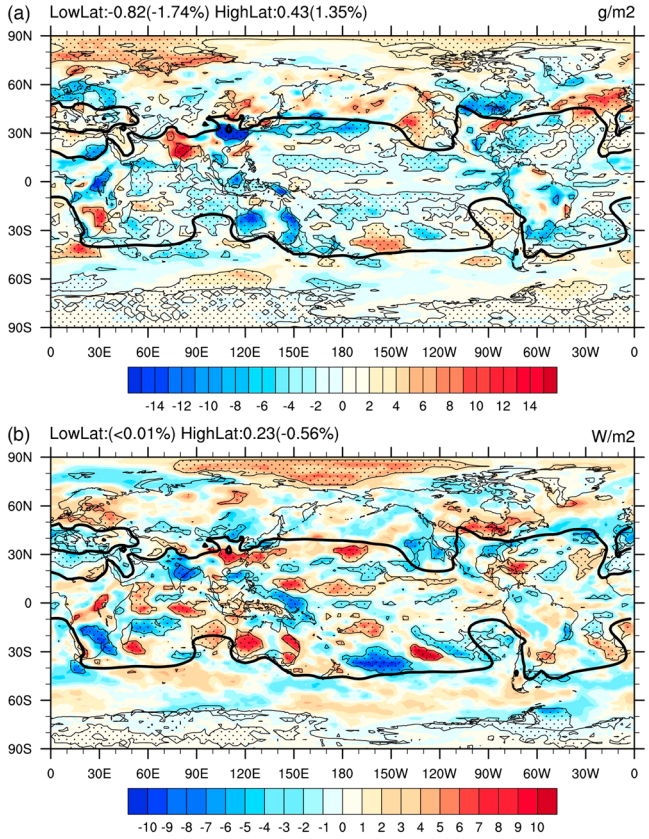

Figure 9. (a) Global liquid water path difference between the simulation with varying ν and the control simulation of $\nu = 1.0$ (dotted hatch is the area passing the statistical significance test with 95% confidence level). The thick solid line represents the contour of $\nu = 1.0$ in the simulation with varying ν. (b) Same as Figure 9a but for shortwave cloud forcing.

changed which will in turn impact the model hydrological and dynamical processes. We have run CESM in a $2° \times 2°$ resolution for 4 years, and the following analysis is based on the annual mean of the last 3 year results. In the CESM longitude and latitude grid setting, the $2° \times 2°$ resolution corresponds to spatial grid scale ranging from over 200 km near the equator to about 5 km in the polar region. Owing to the interactive nature of the cloud microphysics and radiation, the response is not expected to be the same as the direct impact of ν in the offline simulation.

Figure 9a shows the difference of the annual liquid water path between the simulation with varying ν and the control run with fixed $\nu = 1.0$. The black thick line shows the contour of $\nu = 1.0$. The hatching area passes Student's t test with the confidence level 95%. It is seen that even though the interactive response is very noisy, at higher latitudes where $\nu > 1.0$, there is an overall increase of cloud liquid water path; in the middle and low latitudes, cloud liquid water is overall reduced. We have calculated the area average of these differences in both high latitudes (poleward of 45°) and low latitudes (equatorward of 45°). The area-averaged liquid water path is increased by 0.43 g/m^2 in high latitudes and decreased by 0.82 g/m^2 in low latitudes. These represent about 1.4% increase and 1.7% decrease of the cloud water path in the control simulations.

The distribution change of liquid water content is expected to impact radiation. Because the parameterization in this study only affects warm liquid clouds, the radiative impact is expected to be most clear in the regions of low clouds. Figure 9b shows the shortwave cloud forcing difference between varying ν and control $\nu = 1$. The local response is generally consistent with the liquid cloud content change, where liquid increase (decrease) implies stronger (weaker) shortwave cloud forcing. While the figure is noisy, in the subtropical eastern Pacific where low clouds dominate and ν is larger than 1, shortwave cloud forcing is more negative. The difference is about 5 W/m^2. When averaged over the globe, the varying ν has relatively small impact on the overall climate, so its influence on other fields is not shown. This suggests that the default model is nearly optimally tuned. However, the impact of the parameterized ν on a model with different resolution may be larger if the shape parameter is not optimally tuned.

5. Conclusions

We analyzed the long-term ground-based MICROBASE data set to derive the liquid cloud inhomogeneity represented by the shape parameter ν of the gamma distribution. Smaller ν is associated with larger inhomogeneity. We reported the dependence of ν on the horizontal scale and atmospheric instability and derived a scale-aware parameterization of ν that depends on the model resolution and atmospheric state.

When the parameterization is implemented in CESM at a $2° \times 2°$ resolution, we found that the inhomogeneity parameter ν is larger than the default value of $\nu = 1$ in high latitudes and smaller than the default value in low

latitudes that is used in CESM, owing to the varying grid sizes and atmospheric instability. Larger values of the parameter are shown to correspond to more cloud liquid water, owing to smaller rate of cloud-to-rain conversion. Smaller values of the parameter ν lead to less cloud water in the simulation. The parameterized inhomogeneity therefore leads to more cloud water in high latitudes. However, the overall impact of the parameterization on the default model is small, owing to the fact the default model used a tuned parameter that is close to the observationally derived values.

This study is only a small step toward the scale-aware description of cloud water inhomogeneity. Future studies should include cloud ice and other hydrometeors. While the impact of the parameterized inhomogeneity on the simulated climate in this study is small, we think that the main benefit of the scheme is its direct use in variable resolution models.

Acknowledgments

We thank the three anonymous reviewers whose comments are very valuable for us to improve the paper. This research is supported by the Major National Basic Research Program of China (973 Program) on Global Change under grant 2010CB951800. Additional support is provided by the Biological and Environmental Research Division in the Office of Sciences of the U.S. Department of Energy (DOE) and by National Science Foundation to the Stony Brook University. All data used in this paper are available upon request (email: xin.xie@stonybrook.edu).

References

Arakawa, A., and W. H. Schubert (1974), Interaction of a cumulus cloud ensemble with the large-scale environment: Part I, *J. Atmos. Sci.*, *31*(3), 674–701, doi:10.1175/1520-0469(1974)031<0674:IOACCE>2.0.CO;2.

Barker, H. W. (1996), A parameterization for computing grid-averaged solar fluxes for inhomogeneous marine boundary layer clouds: 1. Methodology and homogeneous biases, *J. Atmos. Sci.*, *53*(16), 2289–2303, doi:10.1175/1520-0469(1996)053<2289:Apfcga>2.0.Co;2.

Barker, H. W., B. A. Wielicki, and L. Parker (1996), A parameterization for computing grid-averaged solar fluxes for inhomogeneous marine boundary layer clouds: 2. Validation using satellite data, *J. Atmos. Sci.*, *53*(16), 2304–2316, doi:10.1175/1520-0469(1996)053<2304:Apfcga>2.0.Co;2.

Bogenschutz, P. A., and S. K. Krueger (2013), A simplified PDF parameterization of subgrid-scale clouds and turbulence for cloud-resolving models, *J. Adv. Model. Earth Syst.*, *5*, 195–211, doi:10.1002/jame.20018.

Boutle, I. A., S. J. Abel, P. G. Hill, and C. J. Morcrette (2013), Spatial variability of liquid cloud and rain: Observations and microphysical effects, *Q. J. R. Meteorol. Soc.*, *140*, 583–594, doi:10.1002/qj.2140.

Cahalan, R. F., W. Ridgway, W. J. Wiscombe, T. L. Bell, and J. B. Snider (1994), The albedo of fractal stratocumulus clouds, *J. Atmos. Sci.*, *51*(16), 2434–2455, doi:10.1175/1520-0469(1994)051<2434:TAOFSC>2.0.CO;2.

Gent, P. R., et al. (2011), The Community Climate System Model version 4, *J. Clim.*, *24*(19), 4973–4991, doi:10.1175/2011JCLI4083.1.

Golaz, J.-C., V. E. Larson, and W. R. Cotton (2002), A PDF-based model for boundary layer clouds. Part I: Method and model description, *J. Atmos. Sci.*, *59*(24), 3540–3551, doi:10.1175/1520-0469(2002)059<3540:APBMFB>2.0.CO;2.

Grützun, V., J. Quaas, C. J. Morcrette, and F. Ament (2013), Evaluating statistical cloud schemes: What can we gain from ground-based remote sensing?, *J. Geophys. Res. Atmos.*, *118*, 10,507–510,517, doi:10.1002/jgrd.50813.

Hill, P. G., R. J. Hogan, J. Manners, and J. C. Petch (2012), Parametrizing the horizontal inhomogeneity of ice water content using CloudSat data products, *Q. J. R. Meteorol. Soc.*, *138*(668), 1784–1793, doi:10.1002/qj.1893.

Hogan, R. J., and A. J. Illingworth (2003), Parameterizing ice cloud inhomogeneity and the overlap of inhomogeneities using cloud radar data, *J. Atmos. Sci.*, *60*(5), 756–767, doi:10.1175/1520-0469(2003)060<0756:PICIAT>2.0.CO;2.

Huang, D., and Y. Liu (2014), Statistical characteristics of cloud variability. Part II: Implication for parameterizations of microphysical and radiative transfer processes in climate models, *J. Geophys. Res. Atmos.*, *119*, 10,829–10,843, doi:10.1002/2014JD022003.

Huang, D., E. Campos, and Y. Liu (2014), Statistical characteristics of cloud variability. Part I: Retrieved cloud liquid water path at three ARM sites, *J. Geophys. Res. Atmos.*, *119*, 10,813–10,828, doi:10.1002/2014JD022001.

Jakob, C., and S. A. Klein (1999), The role of vertically varying cloud fraction in the parametrization of microphysical processes in the ECMWF model, *Q. J. R. Meteorol. Soc.*, *125*(555), 941–965, doi:10.1002/qj.49712555510.

Jakob, C., and S. A. Klein (2000), A parametrization of the effects of cloud and precipitation overlap for use in general-circulation models, *Q. J. R. Meteorol. Soc.*, *126*(568), 2525–2544, doi:10.1002/qj.49712656809.

Jess, S., P. Spichtinger, and U. Lohmann (2011), A statistical subgrid-scale algorithm for precipitation formation in stratiform clouds in the ECHAM5 single column model, *Atmos. Chem. Phys. Discuss.*, *11*(3), 9335–9374, doi:10.5194/acpd-11-9335-2011.

Johnson, K., and M. Jensen (2011), Atmospheric Radiation Measurement (ARM) Climate Research Facility, Continuous Baseline Microphysical Retrieval (MICROBASEPI2), SGP C1, NSA C1, TWP C3, 2008 to 2010, doi:10.5439/1034923.

Johnson, K., M. Dunn, and M. Jensen (2011), The microbase value-added product: A baseline retrieval of cloud microphysical properties Rep Atmospheric Radiation Measurement Climate Research Facility.

Kawai, H., and J. Teixeira (2011), Probability density functions of liquid water path and total water content of marine boundary layer clouds: Implications for cloud parameterization, *J. Clim.*, *25*(6), 2162–2177, doi:10.1175/JCLI-D-11-00117.1.

Khairoutdinov, M., and Y. Kogan (2000), A new cloud physics parameterization in a large-eddy simulation model of marine stratocumulus, *Mon. Weather Rev.*, *128*(1), 229–243, doi:10.1175/1520-0493(2000)128<0229:Ancppi>2.0.Co;2.

Larson, V. E., and B. M. Griffin (2013), Analytic upscaling of a local microphysics scheme. Part I: Derivation, *Q. J. R. Meteorol. Soc.*, *139*(670), 46–57, doi:10.1002/qj.1967.

Larson, V. E., and J.-C. Golaz (2005), Using probability density functions to derive consistent closure relationships among higher-order moments, *Mon. Weather Rev.*, *133*(4), 1023–1042, doi:10.1175/MWR2902.1.

Lebsock, M., H. Morrison, and A. Gettelman (2013), Microphysical implications of cloud-precipitation covariance derived from satellite remote sensing, *J. Geophys. Res. Atmos.*, *118*, 6521–6533, doi:10.1002/jgrd.50347.

Morrison, H., and A. Gettelman (2008), A new two-moment bulk stratiform cloud microphysics scheme in the Community Atmosphere Model, version 3 (CAM3). Part I: Description and numerical tests, *J. Clim.*, *21*(15), 3642–3659, doi:10.1175/2008jcli2105.1.

Norris, P. M., L. Oreopoulos, A. Y. Hou, W.-K. Tao, and X. Zeng (2008), Representation of 3D heterogeneous cloud fields using copulas: Theory for water clouds, *Q. J. R. Meteorol. Soc.*, *134*(636), 1843–1864, doi:10.1002/qj.321.

Oreopoulos, L., and R. F. Cahalan (2005), Cloud inhomogeneity from MODIS, *J. Clim.*, *18*(23), 5110–5124, doi:10.1175/Jcli3591.1.

Pincus, R., and S. A. Klein (2000), Unresolved spatial variability and microphysical process rates in large-scale models, *J. Geophys. Res.*, *105*(D22), 27,059–27,065, doi:10.1029/2000JD900504.

Pincus, R., and B. Stevens (2009), Monte Carlo spectral integration: A consistent approximation for radiative transfer in large eddy simulations, *J. Adv. Model. Earth Syst.*, *1*, doi:10.3894/JAMES.2009.1.1.

Pincus, R., S. A. McFarlane, and S. A. Klein (1999), Albedo bias and the horizontal variability of clouds in subtropical marine boundary layers: Observations from ships and satellites, *J. Geophys. Res.*, *104*(D6), 6183–6191, doi:10.1029/1998JD200125.

Pincus, R., H. W. Barker, and J.-J. Morcrette (2003), A fast, flexible, approximate technique for computing radiative transfer in inhomogeneous cloud fields, *J. Geophys. Res.*, *108*(D13), 4376, doi:10.1029/2002JD003322.

Pincus, R., R. Hemler, and S. A. Klein (2006), Using stochastically generated subcolumns to represent cloud structure in a large-scale model, *Mon. Weather Rev.*, *134*(12), 3644–3656, doi:10.1175/MWR3257.1.

Raisanen, P., H. W. Barker, M. F. Khairoutdinov, J. N. Li, and D. A. Randall (2004), Stochastic generation of subgrid-scale cloudy columns for large-scale models, *Q. J. R. Meteorol. Soc.*, *130*(601), 2047–2067, doi:10.1256/Qj.03.99.

Shonk, J. K. P., and R. J. Hogan (2008), Tripleclouds: An efficient method for representing horizontal cloud inhomogeneity in 1D radiation schemes by using three regions at each height, *J. Clim.*, *21*(11), 2352–2370, doi:10.1175/2007JCLI1940.1.

Shonk, J. K. P., and R. J. Hogan (2010), Effect of improving representation of horizontal and vertical cloud structure on the Earth's global radiation budget. Part II: The global effects, *Q. J. R. Meteorol. Soc.*, *136*(650), 1205–1215, doi:10.1002/qj.646.

Shonk, J. K. P., R. J. Hogan, J. M. Edwards, and G. G. Mace (2010), Effect of improving representation of horizontal and vertical cloud structure on the Earth's global radiation budget. Part I: Review and parametrization, *Q. J. R. Meteorol. Soc.*, *136*(650), 1191–1204, doi:10.1002/qj.647.

Taylor, M. A., J. Edwalrds, and A. S. Cyr (2008), Petascale atmospheric models for the Community Climate System Model: New developments and evaluation of scalable dynamical cores, *J. Phys. Conf. Ser.*, *125*, 12,023–12,023, doi:10.1088/1742-6596/125/1/012023.

Thom, H. C. S. (1958), A note on the gamma distribution, *Mon. Weather Rev.*, *86*(4), 117–122, doi:10.1175/1520-0493(1958)086<0117:ANOTGD>2.0.CO;2.

Tompkins, A. M. (2002), A prognostic parameterization for the subgrid-scale variability of water vapor and clouds in large-scale models and its use to diagnose cloud cover, *J. Atmos. Sci.*, *59*(12), 1917–1942, doi:10.1175/1520-0469(2002)059<1917:APPFTS>2.0.CO;2.

Weber, T., and J. Quaas (2012), Incorporating the subgrid-scale variability of clouds in the autoconversion parameterization using a PDF-scheme, *J. Adv. Model. Earth Syst.*, *4*, M11003, doi:10.1029/2012MS000156.

Wood, R., P. R. Field, and W. R. Cotton (2002), Autoconversion rate bias in stratiform boundary layer cloud parameterizations, *Atmos. Res.*, *65*(1–2), 109–128, doi:10.1016/S0169-8095(02)00071-6.

Xie, S., et al. (2010), Clouds and more: ARM climate modeling best estimate data, *Bull. Am. Meteorol. Soc.*, *91*(1), 13–20, doi:10.1175/2009BAMS2891.1.